Supporting Information

Gilles Argouarch,*[,†] Guillaume Grelaud,[†,‡] Thierry Roisnel,[§] Mark G. Humphrey,*[,‡] and Frédéric Paul*[,†]

[Fp*Fc][PF6]; A Remarkable Non-symmetric DinuclearCation in a Very Stable Mixed-Valent State

Including:

† Institut des Sciences Chimiques de Rennes.

‡ Research School of Chemistry.

§ Centre de Diffractométrie X, Rennes.

1. Crystallographic Section

Table S1. Collection Parameters for 2[PF_6]

compound	**2[PF_6]**
formula	$C_{22}H_{24}F_6Fe_2O_2P$
fw	577.08
space group	*P* $2_1/m$
a, Å	7.4396(7)
b, Å	14.1414(11)
c, Å	10.8993(11)
α, deg	90
β, deg	94.108(3)
γ, deg	90
V, $Å^3$	1143.73(18)
Z	2
d_{calcd}, g/cm^3	1.676
θ range, deg	2.74–27.49
μ, mm^{-1}	1.405
no. of obsd data, $I > 2\sigma(I)$	2362
data / restraints / parameters	2705 / 0 / 163
R1 (all data)[a]	0.0345
wR2 (all data)[b]	0.0755
$(\Delta\rho)_{min}$, $e.Å^{-3}$	–0.377
$(\Delta\rho)_{max}$, $e.Å^{-3}$	0.445

[a] $R1 = \sum | |F_o| - |F_c| | / \sum |F_o|$. [b] $wR2 = \{\sum [w(F_o^2 - F_c^2)^2] / \sum [w(F_o^2)^2]\}^{1/2}$.

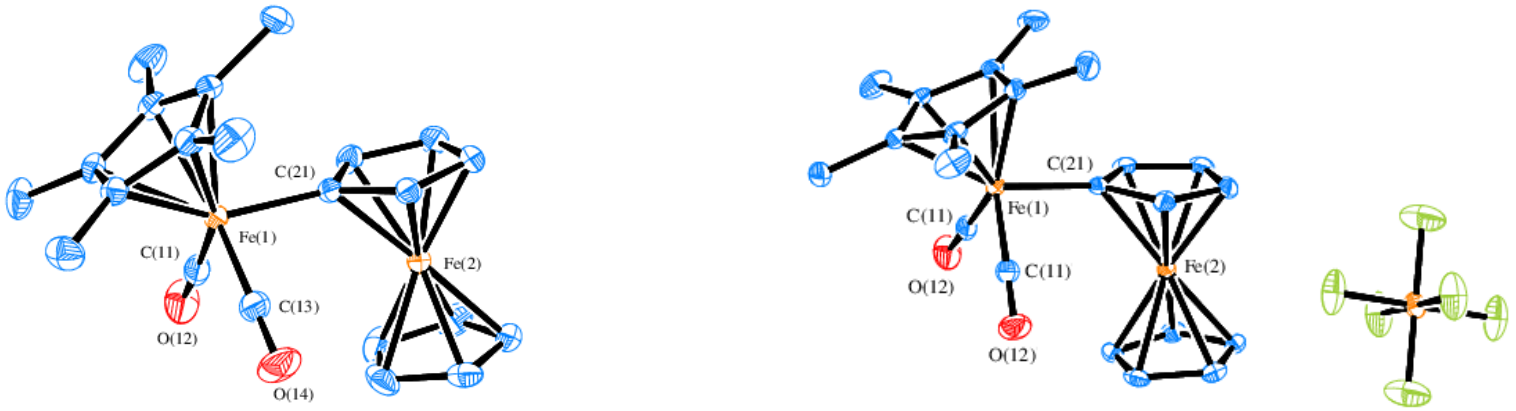

2 **2**[PF_6]

Figure S1. Comparative molecular diagrams of compounds **2** and **2**[PF_6] at the 40% probability level. All hydrogen atoms have been omitted for clarity. Selected bond distances (Å) and angles (deg): **2,** Fe(1)–C(11) 1.752(2), Fe(1)–C(13) 1.760(2), Fe(1)–C(21) 1.985(0), C(11)–O(12) 1.152(2), C(13)–O(14) 1.148(2), Fe(1)–$Cp^*_{centroid}$ 1.729, Fe(2)–$Cp_{centroid}$ 1.653, C(11)–Fe(1)–C(13) 96.48(9), C(11)–Fe(1)–C(21) 90.57(8), C(13)–Fe(1)–C(21) 90.81(8), O(12)–C(11)–Fe(1) 177.2(5), O(14)–C(13)–Fe(1) 177.7(4), C(21)–Fe(1)–$Cp^*_{centroid}$ 120.31, C(11)–Fe(1)–$Cp^*_{centroid}$ 124.58, C(13)–Fe(1)–$Cp^*_{centroid}$ 124.74. **2**[PF_6], Fe(1)–C(11) 1.766(2), Fe(1)–C(21) 1.964(2), C(11)–O(12) 1.145(2), Fe(1)–$Cp^*_{centroid}$ 1.736, Fe(2)–$Cp_{centroid}$ 1.715, C(11)–Fe(1)–C(11) 96.00(1), C(11)–Fe(1)–C(21) 92.33(8), O(12)–C(11)–Fe(1) 178.60(1), C(21)–Fe(1)–$Cp^*_{centroid}$ 119.77, C(11)–Fe(1)–$Cp^*_{centroid}$ 124.04.

2. Cyclic Voltammetry

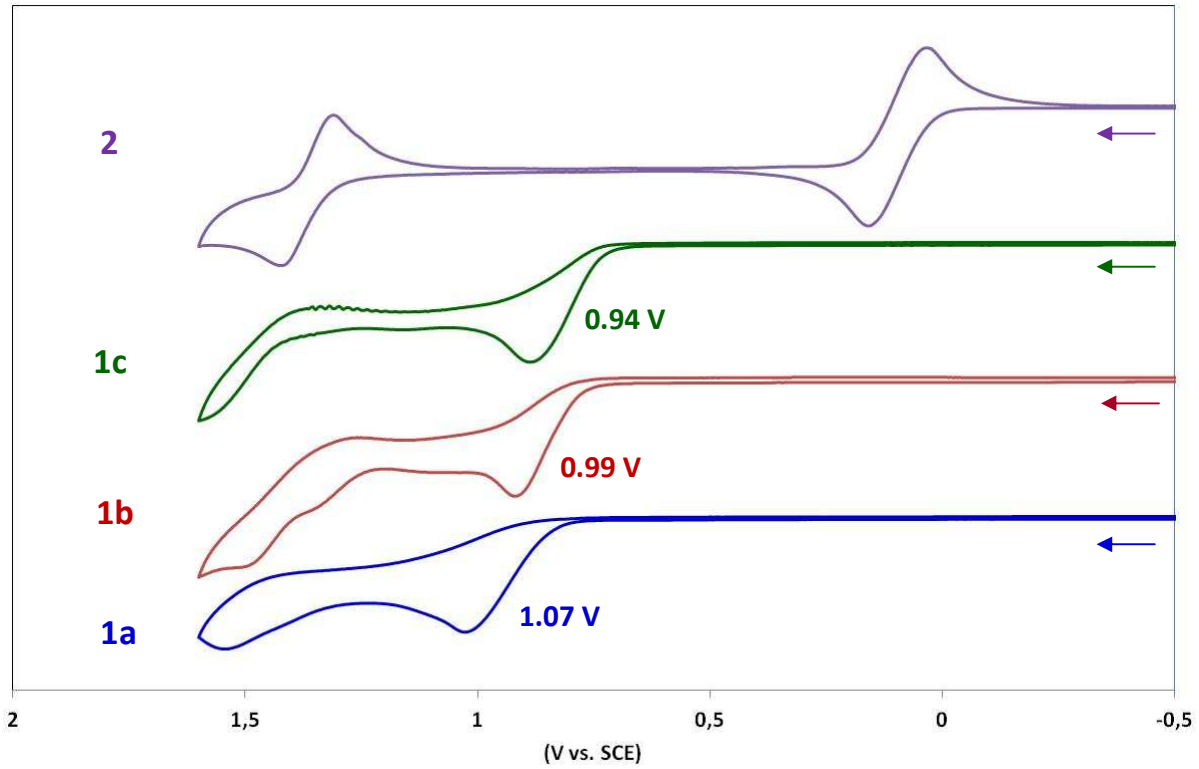

Figure S2. Voltammograms of **1a-c** and **2** in CH_2Cl_2 ($[Bu_4N][PF_6]$, 0.1 M, 25°C, scan rate: 0.12 $V.s^{-1}$; E° (FcH^+/FcH) = +0.46 V vs. SCE).

3. Mössbauer Spectroscopy

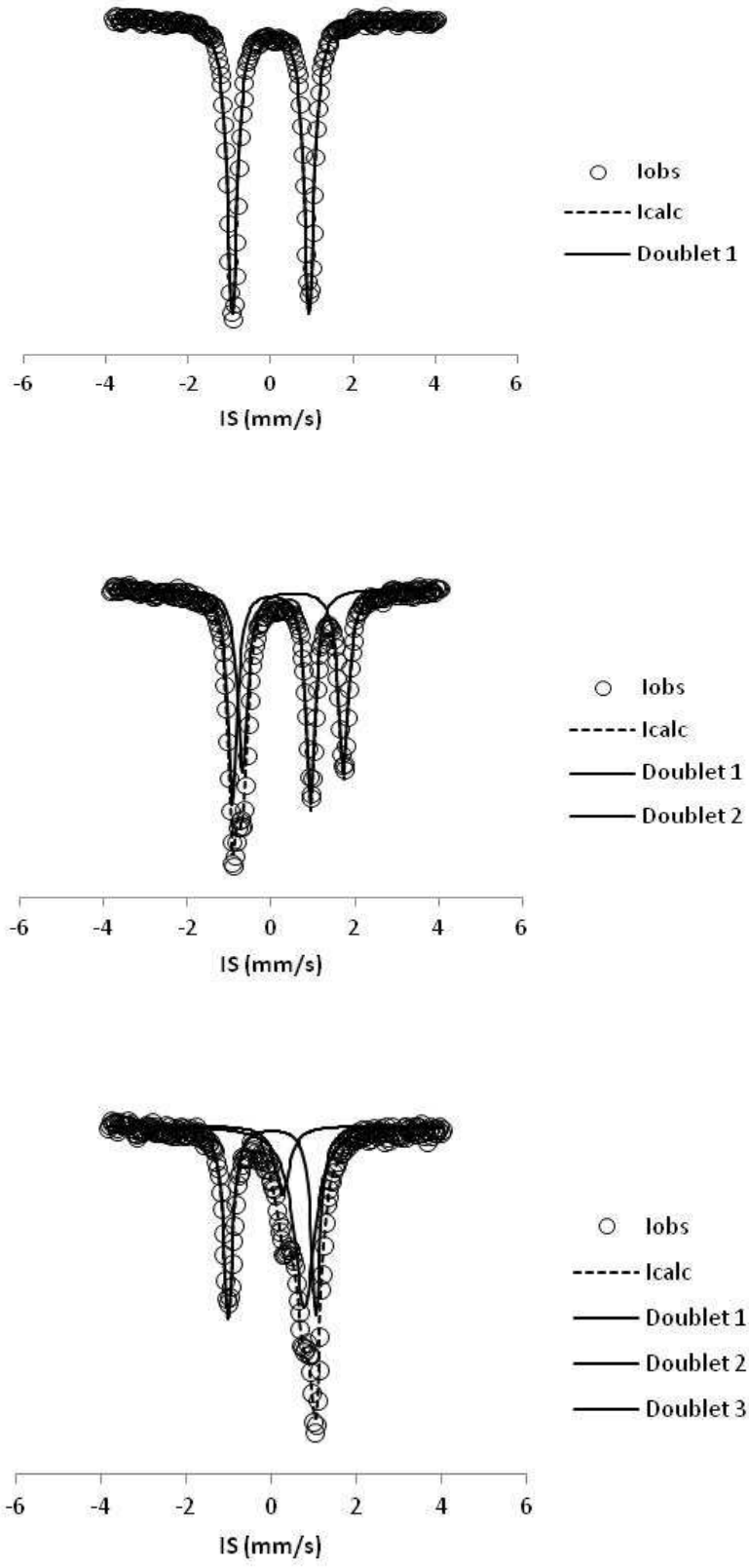

Figure S3. Mössbauer spectra of **1a** (upper), **2** (middle) and **2**[PF_6] (bottom) at 80 K.

Table S2. ^{57}Fe Mössbauer Fitting Parameters at 80 K for Selected Complexes.

Compd	δ^a	$\Delta E_Q{}^b$	Γ^c	% area ^{d}
		(mm.s^{-1})		
1a	0.00605(98)	1.8607(20)	0.1484(15)	100
2	0.0149(14)	1.8587(27)	0.1314(21)	51.9
	0.5266(17)	2.4068(34)	0.1433(27)	48.1
2[PF_6]	0.0257(27)	2.0257(27)	0.1271(40)	41.7
	0.7878(93)	0	0.294(15)	46.3
	0.268(15)	0	0.198(42)	12.0

^{a} Isotropic shifts (IS) of the various doublets. ^{b} Quadrupolar separations (QS) of the various doublets. ^{c} Halfwidth of the various peaks. ^{d} Percentage of each doublet *vs.* total area.

The Mössbauer spectrum of **2** at 80 K can be fitted by two doublets. The former (QS ≈ 1.859, IS ≈ 0.015 mm.s^{-1}) most likely correspond to the Fe(II) atom of the Fp* site by comparison with **1a** (QS ≈ 1.861, IS ≈ 0.006 mm.s^{-1}), while the second (QS ≈ 2.407, IS ≈ 0.527 mm.s^{-1}) is assigned to the Fe(II) atom of the ferrocenyl moiety, since the QS value is typical for substituted ferrocene.[29] After oxidation, the Mössbauer spectrum of **2**[PF_6] at the same temperature can be fitted by two new doublets of nearly the same intensity. The first of these (QS ≈ 2.062, IS = 0.027 mm.s^{-1}) quite certainly corresponds to Fe(II) atoms of the Fp* site, while the other one of similar intensity is now a collapsed doublet (QS = 0, IS = 0.788 mm.s^{-1}) typical of Fe(III) atoms in ferrocenium sites.[29, 30] The slight changes observed for the IS and QS values of the Fe(II) atom of the Fp* site between **2** and **2**[PF_6] could reflect the increased weight of resonance form B after oxidation. To complete this fit, an additional but much weaker contribution must also be considered (QS = 0; IS = 0.268 mm.s^{-1}). The origin of that singlet peak remains unclear yet.

4. ^{1}H NMR and ESR of **2**[PF_6]

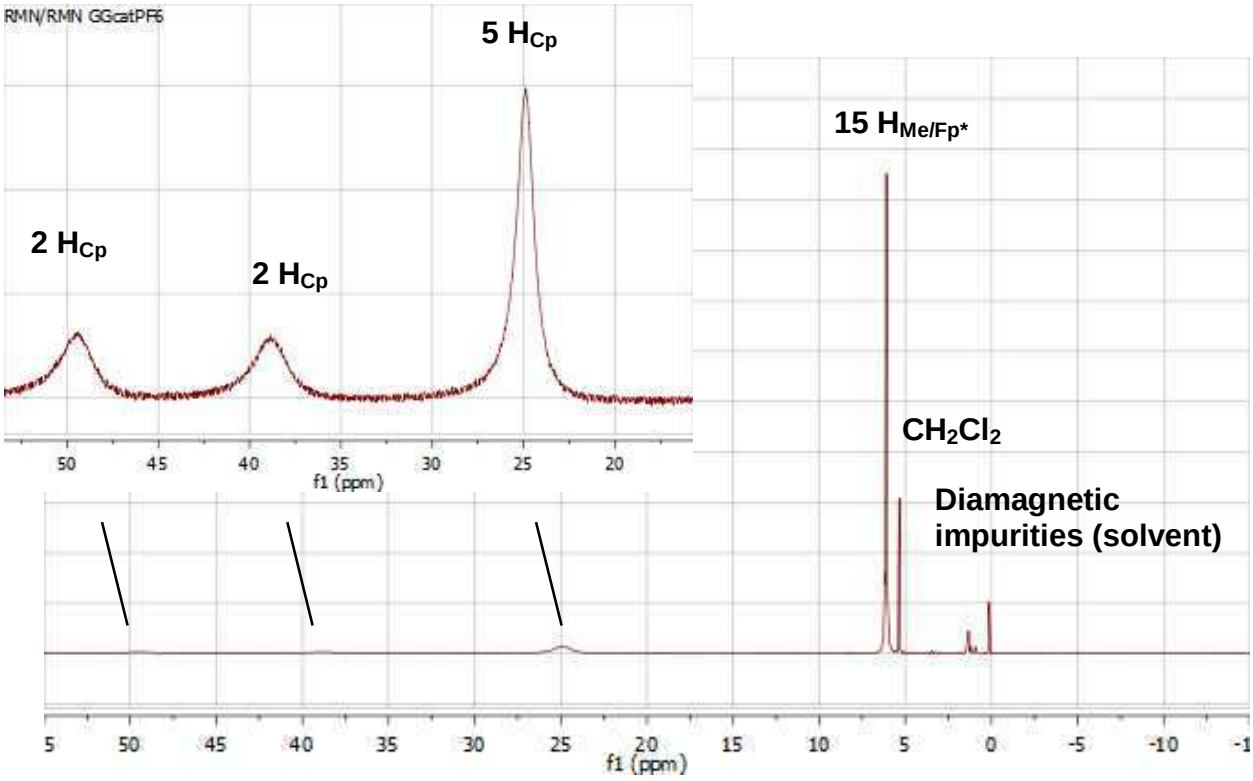

Figure S4. ^{1}H NMR spectra of **2**[PF_6] in CD_2Cl_2 at 300 K, with proposed assignment of selected protons**.**

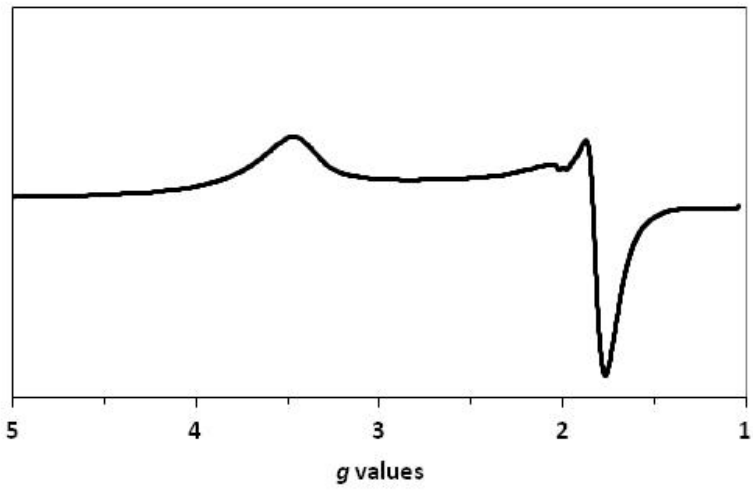

Figure S5. ESR spectrum of **2**[PF_6] in CH_2Cl_2/1,2-$C_2H_4Cl_2$ (1:1) at 80 K.

5. Optical Absorption Studies of 1a-c and 2

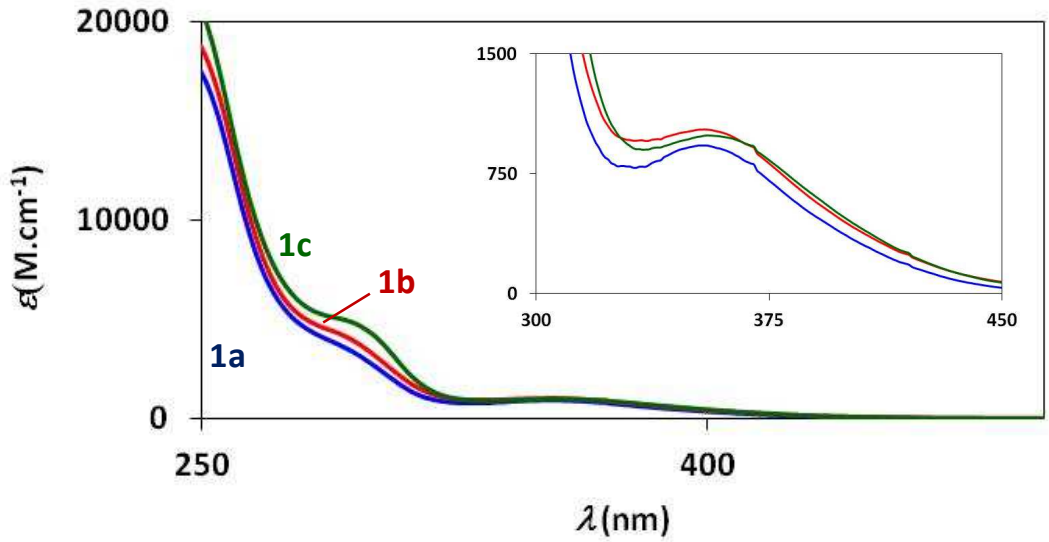

Figure S6. UV-vis Spectra of **1a-c** in CH_2Cl_2. Insert: Expansion of the 300-450 nm spectral range.

Dicarbonyl(pentamethylcyclopentadienyl)phenyliron (1a). UV-Vis (CH_2Cl_2): λ_{max}(ε/10^3 $M^{-1}.cm^{-1}$) = 287 (sh, 4.00), 354 (sh, 0.93).

Dicarbonyl(pentamethylcyclopentadienyl)(4-methylphenyl)iron (1b). UV-Vis (CH_2Cl_2): λ_{max}(ε/10^3 $M^{-1}.cm^{-1}$) = 286 (sh, 4.60), 354 (sh, 1.02).

Dicarbonyl(pentamethylcyclopentadienyl)(4-methoxyphenyl)iron (1c). UV-Vis (CH_2Cl_2): λ_{max}(ε/10^3 $M^{-1}.cm^{-1}$) = 289 (sh, 5.08), 356 (sh, 0.99).

Dicarbonyl(pentamethylcyclopentadienyl)ferroceniumyliron (2). UV-Vis (CH_2Cl_2): λ_{max}(ε/10^3 $M^{-1}.cm^{-1}$) = 244 (sh, 19.5), 276 (sh, 9.5), 358 (2.1), 440 (sh, 0.6).

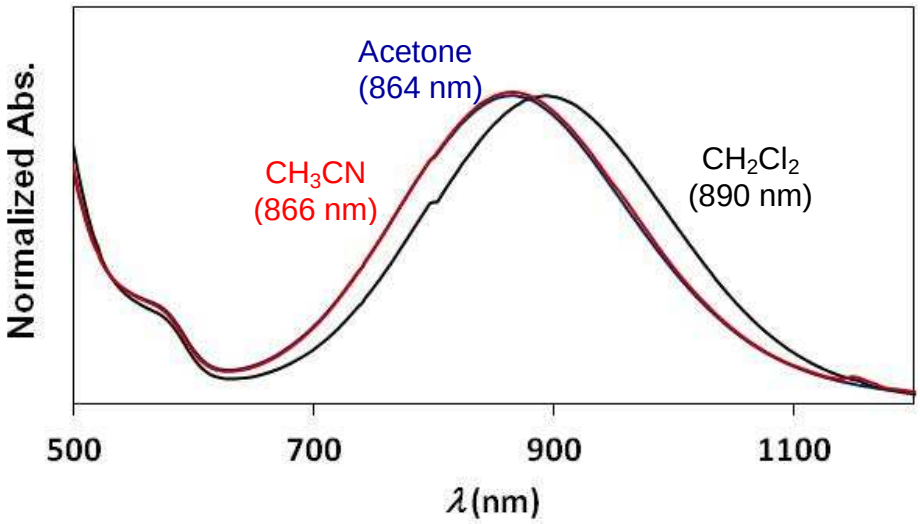

Figure S7. Solvatochromy of the IVCT band of **2**[PF_6] in CH_2Cl_2, Acetone and CH_3CN.

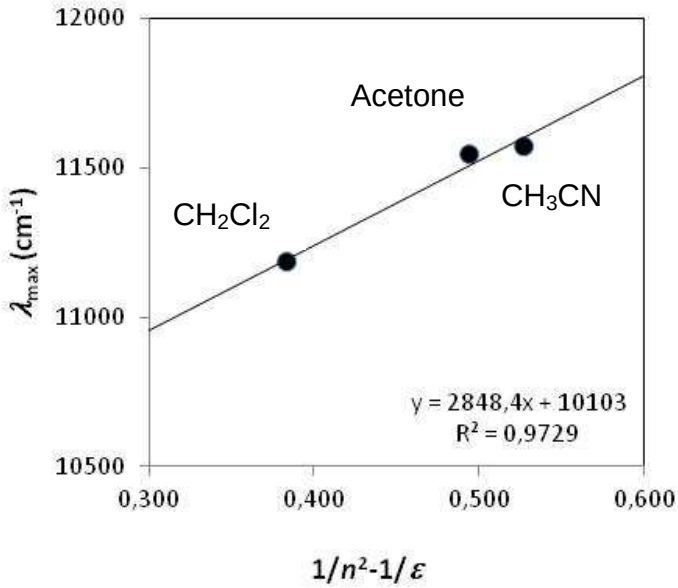

Figure S8. Plot of λ_{max} for the IVCT band of **2**[PF_6] *vs.* $1/n^2 - 1/\varepsilon$ where n is the refractive index of the solvent and ε its relative dielectric constant.

6. Details about the Determination of the Electronic Coupling in 2[PF_6]

According to the Hush model applied to class II unsymmetrical MV complexes (eq. 3), the theoretical bandwidth of an IVCT transition is related to ΔG^0, the energy gap between the two potential wells corresponding to the two diabatic redox states represented by the VB mesomers **A** and **C** (Scheme 2) on the reaction coordinate axis, and to $\bar{\upsilon}_{max}$, the energy of the peak maximum.[12] For **2**[PF_6], this quantity (ΔG^0) was estimated from the difference in the oxidation potentials of the monomeric model complexes ferrocene and **1a** in dichloromethane, which amounts to ca. 4470 cm^{-1}. The oxidation potential of **1a** was estimated from the cyclic voltammogram of this compound considering the observed cathodic oxidation peak and the peak-to-peak separation (ΔE_p) observed for ferrocene under similar conditions (0.12 V).[1] As shown in Table S2, the theoretical halfwidth $(\Delta\bar{\upsilon}_{1/2})_{theo}$ of the IVCT computed according to eq. 4 is larger than that found experimentally for curve A [$(\bar{\upsilon}_{1/2})_{exp}$] (Figure 2b). As discussed in the article, this can be attributed to uncertainties in the determination of the actual ΔG^0 value of the system associated with intrinsic limitations of the Hush model.

Assuming that band A (Figure 2b) corresponds to the IVCT transition, the electronic coupling ($H_{MM'}$) found for the MV **2**[PF_6] amounts to 880 ± 10 cm^{-1} (Table S2) when the Fe-Fe ($d_{MM'}$) distance is taken as 3.8 Å, as derived from the crystallographic data available for **2**[PF_6]. When the entropy associated with the solvent reorganization and other exogenous stabilizing factors of the MV state are neglected, an estimate of the reorganization energy λ can be derived (ca. 6830 cm^{-1}) for $\mathbf{2}^+$ using eq. S1 and ΔG^0 (Table S2). This reorganization energy is much larger than twice the electronic coupling ($2H_{MM'} < \lambda$), so these compounds can be considered as class II MV complexes in the classification of Robin and Day.[11] Considering that $2H_{MM'}/\lambda < [1-(\Delta\bar{\upsilon}_{1/2})_{theo}/2\lambda]$, they can be further categorized as class IIA MV compounds according to this criterion in the sub-categorization developed for symmetric MV complexes by Brunschwig and coworkers.[13] In other words, they are strongly-coupled MV complexes

[1] $\Delta G^0 = e\times[E^0_{\mathbf{1a}} - E^0_{\mathbf{FcH}}]$ (in this expression, e represents the charge of the electron).

with a "localized" valency on the NMR time scale in the GS.[14] In line with such a categorization, a hypsochromic shift of the IVCT is stated in more polar solvents (Figure S7) which linearly correlates with the solvent function (Figure S7). [16, 38] The values of the internal reoganization (λ_{in}) that can be extracted by this mean should however be considered with caution given the uncertainty on ΔG^0.

$$\bar{\upsilon}_{max} = \lambda + \Delta G^0 \qquad \text{(S1)}$$

$$\Delta G_{deloc} \approx (H_{MM'})^2/(\lambda + \Delta G^0) \approx (H_{MM'})^2/\bar{\upsilon}_{max} \qquad \text{(S2)}$$

Finally, using eq. S2,[15, 37] an estimate of the contribution of the electronic coupling to the separation between the redox waves ($\Delta E_{deloc} = \Delta G_{deloc}/e$) can be derived from the spectroscopic data available. Values of ca. 0.008 V are found for **2**[PF_6]. In line with our simulation of the diabatic potential curves of this MV system (Figure S9), it is clear that the electronic coupling does not contribute much to the large increase (0.73 V) seen when the difference between the first and second oxidation potentials of **2** (ΔE^0 = 1.28 V) is compared to that between those of the mononuclear model compounds used ($\Delta G^0/e$ = 0.55 V).[1]

Table S3. Near-IR Data for **2**[PF_6].

Band	$\bar{\upsilon}_{max}$ in cm^{-1} [a] (ε in M^{-1} cm^{-1}) [b]	$(\Delta\bar{\upsilon}_{1/2})_{exp}$ (cm^{-1})	ΔG^0 (cm^{-1}) [b]	$(\Delta\bar{\upsilon}_{1/2})_{theo}$ (cm^{-1}) [b,c]	$H_{MM'}$ [a] (cm^{-1})
A	11300 (804)	2914	4468	3972	882 [d,e] / 3415 [e]
B	17600 (180)	2165	4468	5507	/

[Fp*] ≡ Fe(η^5-C_5Me_5)$(CO)_2$ and [Fc] ≡ Fe(η^5-C_5H_5)(η^5-C_5H_4)-. [a] Values ± 50 cm^{-1}. [b] Values ± 10%. [c] Calculated following eq. 4. Note that these values are only appropriate for IVCT bands; they are included here to illustrate the incompatibility of the experimental halfwidth measured for band B and that calculated from the classical Hush model. [d] Calculated following eq. 3 with $d_{MM'}$ = 3.8 Å. [e] Calculated for a class III MV complex ([$\bar{\upsilon}_{max}$-ΔG^0]/2).

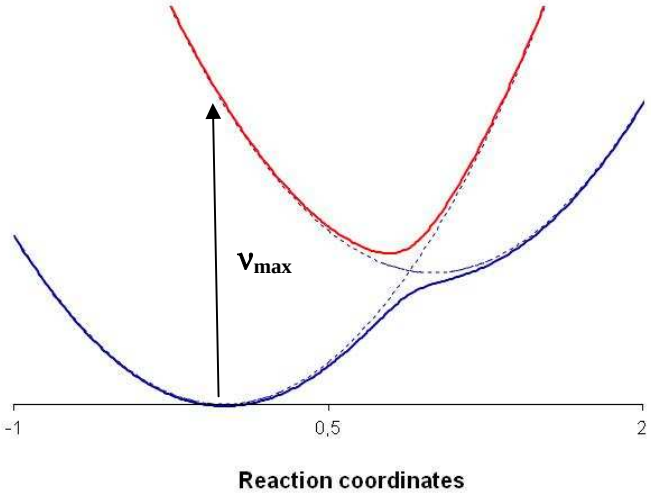

Figure S9. Simulation of the two-state Hush diagram along the electron-transfer pathway using the $H_{MM'}$ and ΔG^0 parameters in Table S3 (band A) and representing the adiabatic ground (blue) and excited (red) states (bold lines) resulting from the coupling of two (localized) diabatic states (dotted lines). The IVCT transition is represented by the arrow ($\bar{\upsilon}_{max}$).